Tracing exciton dynamics in molecular nanotubes with 2D electronic spectroscopy

ARTICLE *in* CHEMICAL PHYSICS LETTERS · JANUARY 2009

Impact Factor: 1.9 · DOI: 10.1016/j.cplett.2008.12.055

Chemical Physics Letters 469 (2009) 130–134

Contents lists available at ScienceDirect

Chemical Physics Letters

journal homepage: www.elsevier.com/locate/cplett

Tracing exciton dynamics in molecular nanotubes with 2D electronic spectroscopy

Alexandra Nemeth [a], Franz Milota [a], Jaroslaw Sperling [a], Darius Abramavicius [b], Shaul Mukamel [b], Harald F. Kauffmann [a,c,*]

[a] Department of Physical Chemistry, University of Vienna, Währingerstrasse 42, A-1090 Vienna, Austria
[b] Department of Chemistry, University of California, Irvine, California 92697-2025, USA
[c] Ultrafast Dynamics Group, Faculty of Physics, Vienna University of Technology, Wiedner Hauptstrasse 8-10, A-1040 Vienna, Austria

ARTICLE INFO

Article history:
Received 6 November 2008
In final form 11 December 2008
Available online 24 December 2008

ABSTRACT

Identifying the pathways and timescales of excitation energy transfer is a central goal in the design of artificial light harvesting systems and energy transporting wires. Coherent femtosecond two-dimensional electronic spectroscopy provides this information for a molecular nanotube by correlating excitonic absorption and emission frequencies at various delay periods. In combination with simulations based on a coupled electronic oscillator model the experiments reveal the electronic coupling pattern and show the various energy transfer pathways into the lowest accessible state.

1. Introduction

Tubular shapes are commonly encountered structural motifs for naturally occurring and synthetically prepared nanomaterials. Examples range from chlorosomes of green bacteria [1], over viral capsid proteins [2], to carbon nanotubes [3]. J-aggregate-forming dyes usually self-assemble into linear chains, but recently, by chemical modification of carbocyanine dyes [4], it has become possible to synthesize cylindrical structures with dimensions similar to those encountered in biology. This bottom-up approach is based on a delicate balance between intermolecular forces, including dispersion forces of the cyanine backbone, and hydrophobic and hydrophilic interactions of the substituents. A scheme for the self-assembling mechanism of the carbocyanine dye C_8O_3 [5] (the system under study in this contribution) is shown in Fig. 1a. In aqueous solution, hydrophobic interactions of the octyl-sidechains facilitate the formation of bilayer sheets, which self-assemble into several μm long cylindrical double-wall structures with typical diameters of approx. 10 nm [6]. The double-walled strands further build up helices in which up to five tubules twist around each other forming a chiral suprastructure. Possible application of these chiral systems as building blocks for artificial light harvesting devices [7] or nanometer-scale wires for energy transport [8] renders the characterization of energy flow pathways and timescales a topic of high interest.

The cylindrical geometry splits the linear absorption of an isolated tubule into two bands oriented parallel and perpendicular to the cylinder axis [9]. The splitting is inversely proportional to the tube diameter, while the red-shift with respect to the monomer transition is a measure for inter-chromophore coupling strengths. For a non-interacting double-wall system one would thus expect four excitonic bands, two parallel and two perpendicular to the cylinder axis. The linear absorption spectrum of C_8O_3 in water (cf. Fig. 1b) exhibits four excitonic bands, three (bands I, II, and IV) polarized parallel to the cylinder axis, whereas band III is polarized perpendicular to the long axis of the cylinder. Changes in the absorption spectrum through the addition of diverse surfactants led to the conclusion that bands I and II correspond to the longitudinally polarized transitions of the inner and the outer cylinder, respectively [10]. The blue-shift of band II with respect to band I in combination with a larger diameter of the outer tube leads to a merging of the two perpendicular transitions associated with the two cylinders into one band (III). We presume that band IV originates from electronic excitations sharing several closely lying tubules [1] in the helical architecture, similar to the collective excitations in chlorosomal stacks (although Ref. [11] attributes band IV not to interaction between tubes but to different arrangements of dye molecules within a single double-walled tubule). The experimental linear absorption and linear dichroism (not shown) spectra can be well reconstructed by a four effective electronic oscillator model, as shown by the red line in Fig. 1b. The absence of information on energy transfer pathways and timescales in linear spectra requires the application of nonlinear techniques for obtaining this kind of knowledge.

Coherent two-dimensional (2D) electronic spectroscopy [12–21] is the only technique that directly reveals electronic couplings and energy transfer pathways in real time. This method overcomes the trade-off between spectral and temporal resolution inherent to nonlinear one-dimensional techniques by mapping coupled exciton states onto off-diagonal signals. In 2D electronic spectroscopy a sequence of three laser pulses stimulates the emission of the third-order photon echo field $E_s^{(3)}(t_1, t_2, t_3)$ which depends on three

* Corresponding author. Address: Department of Physical Chemistry, University of Vienna, Währingerstrasse 42, A-1090 Vienna, Austria. Fax: +43 1 4277 9524.
E-mail address: harald.f.kauffmann@univie.ac.at (H.F. Kauffmann).

0009-2614/$ - see front matter © 2008 Elsevier B.V. All rights reserved.
doi:10.1016/j.cplett.2008.12.055

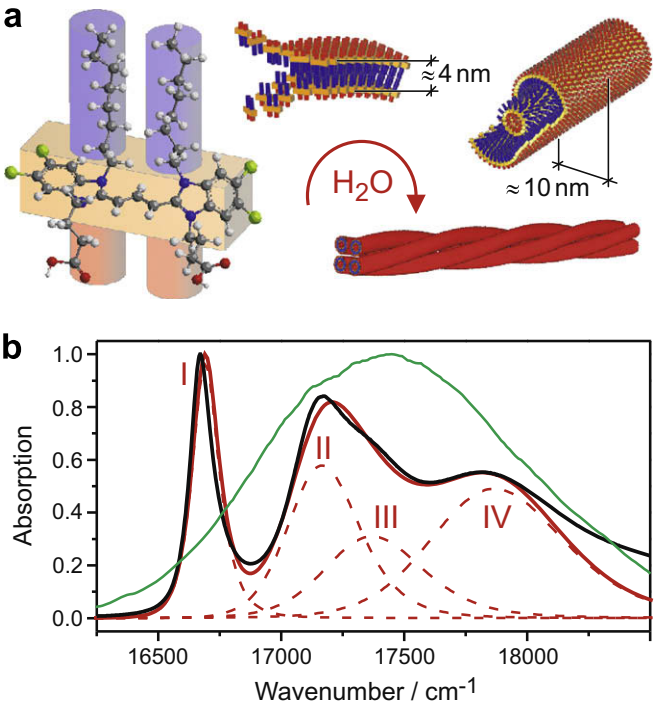

Fig. 1. (a) Schematic of the self-assembling mechanism for building-up the double-wall tubular system C_8O_3 and its chiral suprastructure. The chromophore is depicted in orange, hydrophilic (hydrophobic) sidechains are colored red (blue). (b) The experimental linear absorption spectrum (black line) can be satisfactorily described by four electronic oscillators (dashed red lines indicate their individual contributions, solid red line shows their sum). The laser pulse spectrum is shown as the green envelope.

time delays: t_1 and t_2 being the time delays between pulses 1 and 2, and pulses 2 and 3, respectively, and t_3 denoting the time elapsed after the third pulse (see Fig. 2 of Supplementary material A). Heterodyne-detection with a local oscillator pulse allows for the reconstruction of the electric field amplitude and phase [22]. Fourier transforms of the data with respect to t_1 and t_3 generate the complex-valued 2D frequency-correlation maps $E_s^{(3)}(\omega_1, t_2, \omega_3)$ of the system's response. Diagonal peaks ($|\omega_1| = \omega_3$) in the 2D spectrum resemble linear absorption, whereas off-diagonal contributions ($|\omega_1| \neq \omega_3$) directly reveal couplings between transitions [12]. The cross-peak pattern and its variation with t_2 shows the detailed energy transfer pathways, as was first experimentally demonstrated by Brixner et al. for the photosynthetic FMO complex in the near-infrared spectral region [18].

2. Experimental

Our experiments employ 16 fs pulses centered at 17 500 cm^{-1}. The broad pulse bandwidth (solid green line in Fig. 1b) covers the entire absorption spectrum of C_8O_3. An all-solid state laser system (RegA 9050, Coherent Inc.) pumps a noncollinear optical parametric amplifier (NOPA) [23]. After appropriate compression we routinely achieve sub-20 fs pulses tunable across the visible. To ensure shortest possible pulse durations at the location of the experiment we apply zero-additional-phase spectral phase interferometry for pulse characterization (ZAP-SPIDER) [24]. Heterodyne-detected three-pulse photon echoes are obtained with a diffractive-optics based set-up [16,15,25] and are detected by spectral interferometry. A detailed description of the setup can be found in Refs. [26,27]. Two-dimensional frequency–frequency plots are obtained by scanning time delay t_1, separating the first two interactions of the pulse sequence with the sample, symmetrically around $t_1 = 0$, while delay t_2 between the second and third interaction is kept constant. This scanning procedure collects non-rephasing contributions in the wavevector architecture $\mathbf{k_s} = \mathbf{k_1} - \mathbf{k_2} + \mathbf{k_3}$ for negative values of t_1 and rephasing contributions (true photon echo) in the direction $\mathbf{k_s} = -\mathbf{k_1} + \mathbf{k_2} + \mathbf{k_3}$ for positive t_1 values. Fourier transformation of this data into the ω_1 frequency domain gives purely absorptive real- and purely dispersive imaginary-parts of the 2D spectrum by equally weighting the rephasing and non-rephasing contributions to the signal [28]. t_1-delays are sampled with a resolution of 0.65 fs which is above the Nyquist-frequency dictated by the electronic resonances. To avoid undesired higher-order effects, excitation beams are attenuated to yield less than 3 nJ of energy in each of the excitation

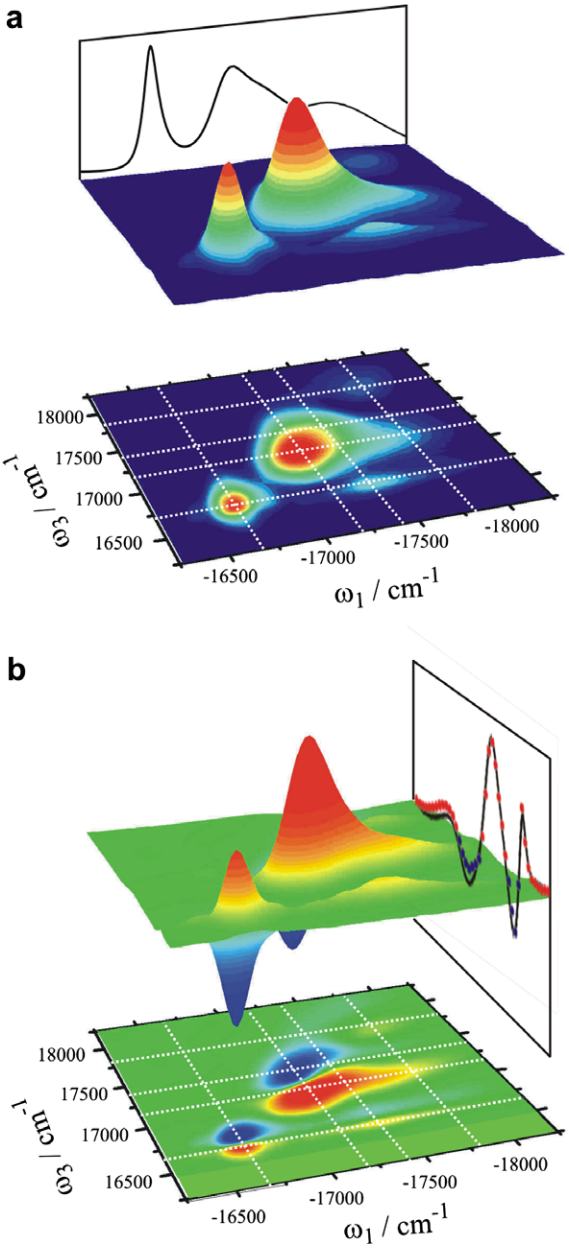

Fig. 2. Amplitude (a) and absorptive part (b) of the 2D electronic correlation ($t_2 = 0$ fs) spectrum of C_8O_3. Both spectra are normalized to their respective maximum absolute value. The linear absorption spectrum is plotted along ω_1 in panel (a), whereas the spectrally resolved pump-probe spectrum (red and blue dots) together with the projection of the absorptive part onto ω_3 (black line) is plotted in panel (b). White dotted lines mark the positions of peak maxima in the linear absorption spectrum.

pulses. This excitation density has been shown to be low enough to exclude annihilation effects from contributing to the detected signal [11]. To eliminate thermal gratings (which can be of the same magnitude as the 3rd-order signals) we have implemented a gravity driven, wire-guided drop jet for the circulation of the sample solution [29,30]. All three excitation beams are polarized perpendicular to the flow of the drop jet. In accordance with the projection slice theorem [13], the real part of all 2D spectra can be phased onto spectrally resolved pump-probe signals with high fidelity, to yield the absorptive and dispersive parts of the complex 2D spectra (cf. Fig. 2b for a comparison of the projected absorptive part to the spectrally resolved pump-probe signal). The carbocyanine-based dye C_8O_3 is obtained commercially (FEW-Chemicals, Germany) and used as received.

3. Results and discussion

The amplitude of the experimental 2D electronic spectrum recorded at a t_2-delay of 0 fs is depicted in Fig. 2a. By comparing the diagonal ($|\omega_1| = \omega_3$) amplitude maxima of the nonlinear signal to the linear absorption (shown along ω_1) we can identify the spectral positions of bands I–IV, as defined in Fig. 1b. The instantaneous observation of off-diagonal features for $t_2 = 0$ fs at all of the possible band-crossings in the $|\omega_1| > \omega_3$ triangular part of the spectrum indicates that all bands are coupled. The most prominent cross-peak at this delay stems from strong correlations between bands I and III, corresponding to the parallel and perpendicular transitions of the inner cylinder, as well as from couplings between band II and IV. The off-diagonal intensities are stretched along ω_1, reflecting a distribution of inter-band coupling strengths between exciton states that share a common ground state.

Upon examination of the absorptive part of the 2D signal, shown in Fig. 2b, we can dissect the various pathways which interfere to form the observed 2D pattern. Positive contributions to the absorptive part originate from ground state bleaching (GSB) and stimulated emission from one-exciton states (SE), negative contributions arise from excited state absorption (ESA) [31]. These two contributions are of equal strength for the diagonal peaks of bands I, II, and III, whereas band IV only shows a weak positive feature. In excitonically coupled systems, ESA is generally blue-shifted with respect to GSB and SE as a direct consequence of the repulsive interaction of Frenkel excitons [32]. The projection of the absorptive part onto the ω_3-axis agrees very well with the spectrally resolved pump-probe signal as shown on the right side of Fig. 2b. Similar to the amplitude spectrum, off-diagonal features are present in the $|\omega_1| > \omega_3$ region of the absorptive part. The observed off-diagonal features are dominated by positive GSB and SE contributions, with ESA signals only having a marginal contribution.

Recording 2D spectra for $t_2 > 0$ fs allows us to directly follow the excitation transfer pathways. As shown in Fig. 3a the relaxation can be divided into three dynamical regimes. Within the first 50 fs the onset of energetic downhill transfer leads to the disappearance of the weak signal of band IV, accompanied by a relative increase of all off-diagonal features in the $|\omega_1| > \omega_3$ triangular region of the spectrum. Population transfer, as controlled by the electronic coupling pattern, causes the transformation of the off-diagonal signals into streak-like shapes, thus mapping out the most efficient relaxation channels. After 200 fs the 2D spectrum is mainly governed by relaxation from states in the vicinity of band III. This causes streaking of band II along ω_1 resolving the coupling between band III and II originally hidden under the intense diagonal peak. After 500 fs we observe relaxation from band II into band I, a process that completes the exciton funneling into the lowest accessible state. As a consequence of the large dimensions of tubular aggregates a microscopic model including disorder needs to incorporate several thousands of coupled chromophores. In order to simulate the experimentally observed features and to quantify relaxation pathways and timescales at a lower cost, we assume an effective level-scheme of single- and double-excited states.

We start with the aggregate model in the basis of products of single-exciton eigenstate space excitations [33], which applies for an arbitrary molecular complex. Each of the four exciton bands is treated as an electronic three-level oscillator, coupled to an overdamped Brownian oscillator [31]. The one- and two-exciton transitions associated with each of the bands I–IV are modeled by

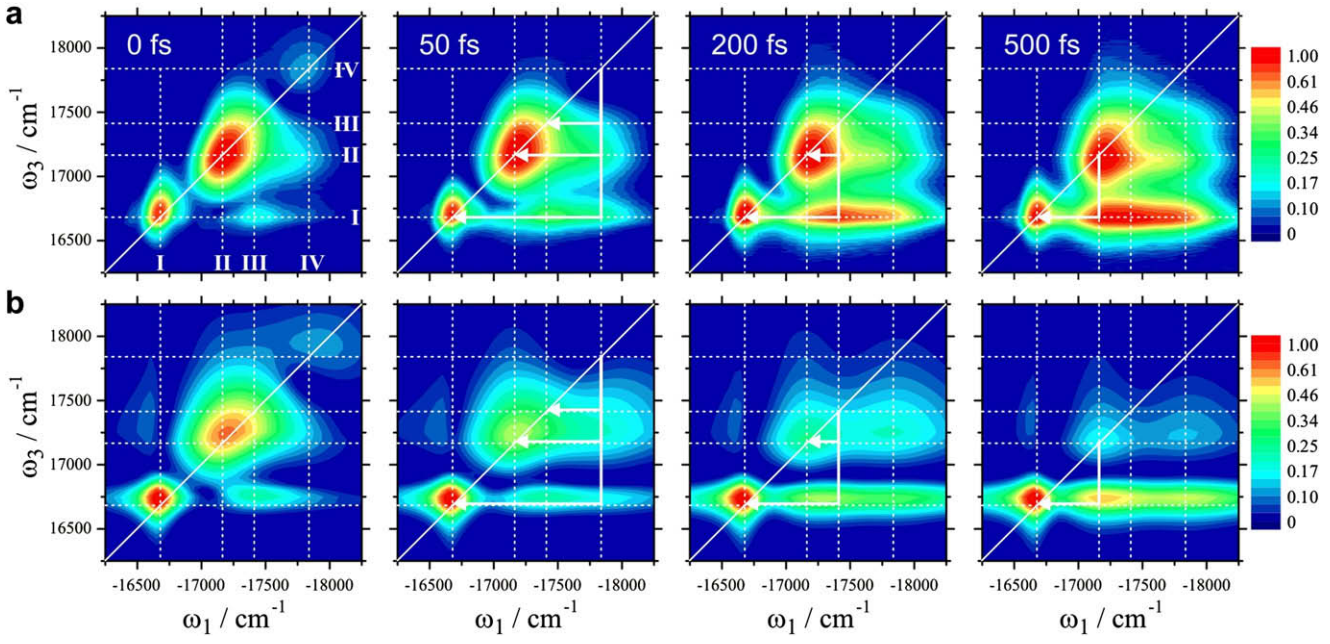

Fig. 3. 2D electronic correlation ($t_2 = 0$ fs) and relaxation ($t_2 > 0$ fs) spectra of C_8O_3. Experimental (a) and simulated (b) amplitude spectra are shown for t_2-delays of 0, 50, 200, and 500 fs. All spectra are normalized to their respective maximum absolute value. White dotted lines indicate the peak positions in the linear absorption spectrum. White arrows mark the main energy transfer pathways.

adjusting the positions and intensities for best match with the linear spectrum, as well as the positive and negative contributions to the diagonal peaks of the absorptive part (cf. Fig. 4). To model off-diagonal signal intensities induced by inter-band couplings, six double-excited states are adjusted as follows. For a particular double-excited state an energetic off-set from the sum of the two single-excitation energies involved is included, which accommodates exciton-repelling interactions and thereby induces a cross-peak. The magnitude of this shift allows to determine the inter-band coupling strengths. Inter-band excitation transfer rates are fitted by simulating the dissipative quantum dynamics using a Pauli master equation. In the global fitting procedure we allow for iterative adjustment of population transfer rates among all of the bands I–IV. As shown in Fig. 3b the dynamic lineshapes can be captured satisfactorily with this procedure. Each of the individual bands transfers population to all lower lying bands with quite similar rates. The results can be summarized by six depopulation time constants of 120 fs (IV–III), 109 fs (IV–II), 192 fs (IV–I), 248 fs (III–II), 229 fs (III–I), and 833 fs (II–I). Fig. 5 shows a schematic representation of these relaxation timescales. Taking into consideration that the excitation energy transfer rates vary over roughly an order of magnitude, it can be concluded that cascading energy transfer pathways play a substantial role in the downhill energy transfer of high energy excitons into the lowest energy band I with intermediate states in the vicinity of band II.

While the simulation recovers the off-diagonal features and their streak-like shapes quite satisfactorily, their intensities deviate from experimental data for longer t_2-delays, particularly in the high energy spectral region which will require a moderate re-adjustment of the model. This difference can be explained by considering that the density of exciton states steeply rises with

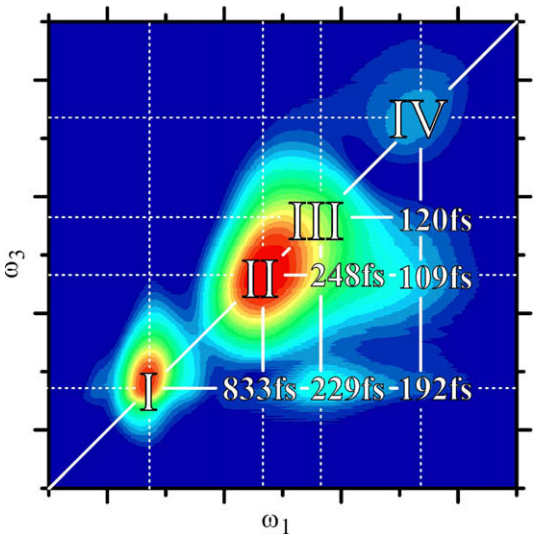

Fig. 5. Schematic representation of relaxation timescales (time constants) as derived from a four band model and an iterative fitting procedure of the experimental data. For intuitive comparison we show the values atop the experimental correlation spectrum. The numerical values in the $|\omega_1| > \omega_3$ triangle of the 2D spectrum are given in femtoseconds (fs) and correspond to the timescales of population transfer *from* a particular band given by the actual column *into* a band given by the corresponding row.

increasing energies as predicted from microscopic models of linear spectral properties of cylindrical J-aggregates [34]. Consequently the assignment of a single effective electronic oscillator to a particular exciton band is only justified in the low energy region where the level density is sparse. At higher energies the average oscillator-strength per state will increasingly differ from the effectively observed transition moment. Furthermore, disorder-induced fluctuations of oscillator-strengths can be expected to lead to an increasing number of weakly absorbing states whose overall contribution to the dynamics cannot be neglected. Finally, this tendency is further enhanced as 2D cross-peaks are proportional to the product of the squared transition dipole magnitudes of both of the states involved in energy transfer ($\propto |\mu_i|^2|\mu_j|^2$). As observed in our experiments, this leads to an increase of cross-peaks as long as one of the states (in our case band I) is a strong absorber, even if the transition moment of the corresponding diagonal signal of the other state is weak.

Before we conclude we want to compare our findings to the results of Ref. [11]. Certainly, the most important finding of Pugzlys et al. as compared to our measurements is a time constant of approx. 275 fs for population transfer from band II to band I, derived from a precursor-successor relation in pump-probe transients. The authors concluded incoherent excitation energy transfer according to Förster's theory. Another conclusion of Ref. [11] is that the inner and outer tubule seem to be only weakly coupled, but the strong off-diagonal features in the experimental 2D spectra of Fig. 3 indicate rather pronounced coupling between the inner and outer tube. Though we observe, so far, no indication of wavelike energy transfer (as has been reported for a natural light harvesting complex at low temperatures [35]), we find a considerable longer time constant (slower rate) of approx. 830 fs for the excitation energy transfer from band II to I (cf. Fig. 5). We believe this to be a consequence of the overlap of bands II and III – which makes a truly selective excitation of band II hardly possible. This finding illustrates the value of multidimensional spectroscopy in relation to other third-order techniques: A selective excitation in pump-probe experiments bears a trade-off in time resolution, while the 2D electronic spectroscopy technique allows to exploit the broad spectral bandwidth

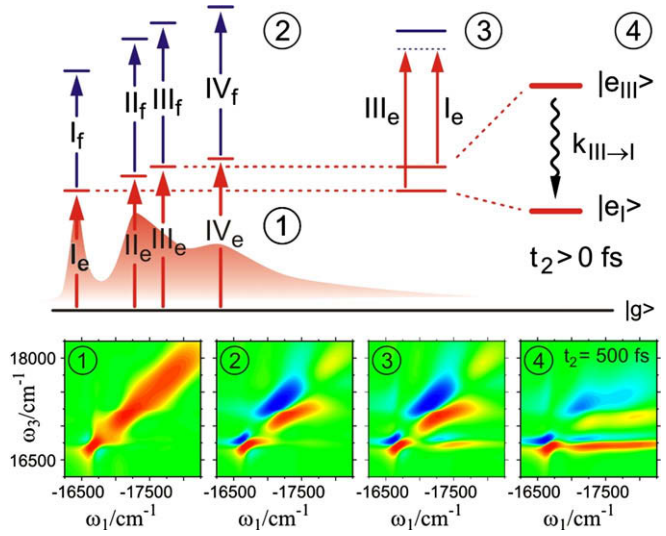

Fig. 4. Stepwise strategy for iterative fitting of the experimental 2D data. (1) Construction of the linear absorption spectrum by assigning transition energies, transition dipole moments, and lineshapes (system-bath coupling strengths) to four single-excited states individually coupled to overdamped Brownian oscillators. This gives an absorptive part 2D spectrum with positive diagonal peaks (lower panel). (2) Four double-excited states are introduced into the effective level-scheme, to account for intra-band one- to two-exciton transitions associated with each of the bands I– IV. (3) Six combination transitions are superimposed on the assembled level structure (schematically depicted for bands I and III in the upper panel) to model off-diagonal signal intensities induced by electronic inter-band couplings. The shift of a particular combination band (blue horizontal solid line) with respect to the sum of the two single-excitation energies involved (blue dotted line), provides a good measure of inter-band coupling strengths. (4) Assignment of inter-band exciton relaxation rates in an iterative fitting procedure. The lower panel shows each step as calculated data, i.e. 1–3 for the correlation spectrum and step 4 for the respective t_2 delay ($t_2 = 500$ fs in this figure).

of sub-20 femtosecond pulses without sacrificing resolution in the frequency domain.

In summary, we have demonstrated highly directed exciton transfer mediated by strong electronic interactions in molecular nanotubes at room temperature. Our study shows how coherent 2D electronic spectroscopy can be used to trace electronic coupling, single-step and sequential band-to-band energy transfer, employing simultaneously high spectral and temporal resolution. The efficient funneling into a single exciton band makes the system an obvious candidate for an artificial light harvesting device.

Acknowledgements

This work was supported by the Austrian Science Foundation (FWF) within the Projects F016-18 (Advanced Light Sources-ADLIS Special Research Program) and P18233. J.S. acknowledges partial funding by the DOC-program of the Austrian Academy of Sciences. S.M. gratefully acknowledges the support of NSF CHE-0745892 and NIH GM-59230.

Appendix A. Supplementary material

Supplementary data associated with this article can be found, in the online version, at doi:10.1016/j.cplett.2008.12.055.

References

[1] V.I. Prokhorenko, D.B. Steensgaard, A.R. Holzwarth, Biophys. J. 85 (2003) 3173.
[2] Y. Xu et al., Chem. Comm. 1 (2008) 49.
[3] P.M. Ajayan, Chem. Rev. 99 (1999) 1787.
[4] A. Pawlik, A. Ouart, S. Kirstein, H.-W. Abraham, S. Dähne, Eur. J. Org. Chem. 16 (2003) 3065.
[5] 1,1′-dioctyl-3,3′-(3-carboxypropyl)-5,5′6,6′-tetrachlorobenzimidacarbocyanine.
[6] H. von Berlepsch, C. Böttcher, A. Ouart, C. Burger, S. Dähne, S. Kirstein, J. Phys. Chem. B 104 (2000) 5255.
[7] T.S. Balaban, Acc. Chem. Res. 38 (2005) 612.
[8] K. Takazawa, Y. Kitahama, Y. Kimura, G. Kido, Nano Lett. 5 (2005) 1293.
[9] C. Didraga, J.A. Klugkist, J. Knoester, J. Phys. Chem. B 106 (2002) 11474.
[10] H. von Berlepsch, S. Kirstein, R. Hania, C. Didraga, A. Pugzlys, C. Böttcher, J. Phys. Chem. B 107 (2003) 14176.
[11] A. Pugzlys, P.R. Hania, R. Augulis, K. Duppen, P.H.M. van Loosdrecht, Int. J. Photoenergy 2006 (2006) 1.
[12] S. Mukamel, Annu. Rev. Phys. Chem. 51 (2000) 691.
[13] D.M. Jonas, Annu. Rev. Phys. Chem. 54 (2003) 425.
[14] P. Tian, D. Keusters, Y. Suzaki, W.S. Warren, Science 300 (2003) 1553.
[15] T. Brixner, T. Mančal, I.V. Stiopkin, G.R. Fleming, J. Chem. Phys. 121 (2004) 4221.
[16] M.L. Cowan, J.P. Ogilvie, R.J.D. Miller, Chem. Phys. Lett. 386 (2004) 184.
[17] C.N. Borca, T. Zhang, X. Li, S.T. Cundiff, Chem. Phys. Lett. 416 (2005) 311.
[18] T. Brixner, J. Stenger, H.M. Vaswani, M. Cho, R.E. Blankenship, G.R. Fleming, Nature 434 (2005) 625.
[19] P. Kjellberg, B. Brüggemann, T. Pullerits, Phys. Rev. B 74 (2006) 024303.
[20] V. Szöcs, T. Palszegi, V. Lukes, J. Sperling, F. Milota, W. Jakubetz, H.F. Kauffmann, J. Chem. Phys. 124 (2006) 124511.
[21] E.M. Grumstrup, S.-H. Shim, M.A. Montgomery, N.H. Damrauer, M.T. Zanni, Opt. Exp. 15 (2007) 16681.
[22] L. Lepetit, M. Joffre, Opt. Lett. 21 (1996) 564.
[23] J. Piel, E. Riedle, L. Gundlach, R. Ernstorfer, R. Eichberger, Opt. Lett. 31 (2006) 1289.
[24] P. Baum, S. Lochbrunner, E. Riedle, Opt. Lett. 29 (2004) 210.
[25] A. Moran et al., J. Chem. Phys. 124 (2006) 194904.
[26] A. Nemeth, F. Milota, T. Mančal, V. Lukeš, H.F. Kauffmann, J. Sperling, Chem. Phys. Lett. 459 (2008) 94.
[27] F. Milota, J. Sperling, A. Nemeth, H.F. Kauffmann, Chem. Phys. (2008), doi:10.1016/j.chemphys.2008.10.015).
[28] M. Khalil, N. Demirdöven, A. Tokmakoff, Phys. Rev. Lett. 90 (2003) 47401.
[29] M.J. Tauber, R.A. Mathies, X. Chen, S.E. Bradforth, Rev. Sci. Instrum. 74 (2003) 4958.
[30] S. Laimgruber, H. Schachenmayr, B. Schmidt, W. Zinth, P. Gilch, Appl. Phys. B 85 (2006) 557.
[31] S. Mukamel, Principles of Nonlinear Optical Spectroscopy, Oxford University Press, Oxford, 1995.
[32] H. Fidder, J. Knoester, D.A. Wiersma, J. Chem. Phys. 98 (1993) 6564.
[33] D. Abramavicius, D.V. Voronine, S. Mukamel, PNAS 105 (2008) 8525.
[34] C. Didraga, J. Knoester, J. Chem. Phys. 121 (2004) 10687.
[35] G.S. Engel et al., Nature 446 (2007) 782.